Semiconductor Science and Technology

PAPER • **OPEN ACCESS**

Short cavity InGaN-based laser diodes with cavity length below 300 μm

To cite this article: Hezhi Zhang *et al* 2019 *Semicond. Sci. Technol.* **34** 085005

OPEN ACCESS
IOP Publishing
Semiconductor Science and Technology
Semicond. Sci. Technol. **34** (2019) 085005 (8pp)
https://doi.org/10.1088/1361-6641/ab2c2f

Short cavity InGaN-based laser diodes with cavity length below 300 μm

Hezhi Zhang, Ching-Wen Shih, Denis Martin, Alexander Caut, Jean-François Carlin, Raphaël Butté and Nicolas Grandjean

École Polytechnique Fédérale de Lausanne (EPFL), Institute of Physics, CH-1015 Lausanne, Switzerland

E-mail: raphael.butte@epfl.ch

Received 10 May 2019, revised 9 June 2019
Accepted for publication 24 June 2019
Published 5 July 2019

Abstract

We report on a practical method for developing InGaN-based edge emitting laser diodes of cavity length down to 45 μm. Samples consisting of one uncoated cleaved facet and one etched facet coated with a high-reflectivity (HR) dielectric distributed Bragg reflector (DBR) exhibit lasing in the continuous wave (cw) regime for cavity lengths down to 250 μm and lasing under pulsed injection for lengths as short as 100 μm. For samples having a second HR dielectric DBR, we could demonstrate cw lasing for a cavity length as short as 45 μm with a threshold current below 10 mA being reported for a 75 μm long device. Through a systematic study of the threshold current (I_{th}) and the slope efficiency (η_s) as a function of cavity length, it is proposed that the parameters underpinning the evolution of I_{th} and η_s with decreasing cavity length and their overall degradation in the short cavity regime are free carrier absorption, Auger processes and the decrease in the recombination losses due to nonuniform carrier distribution across the multiple quantum well active region.

Supplementary material for this article is available online

Keywords: III-nitrides, laser diodes, device processing, short cavities, threshold current, slope efficiency, modal gain

(Some figures may appear in colour only in the online journal)

Introduction

Over the last twenty-five years, III-nitride (III-N) optoelectronics has benefited from tremendous progress, which led to the solid-state lighting revolution [1–3]. Blue to green light-emitting diodes and laser diodes (LDs) became ubiquitous devices used for a wide range of applications. With the need for mobile devices with increased autonomy while offering novel features, there is a demand for low power consumption short-wavelength LDs offering a moderate output power for handheld pico-projection. In order to fulfill such requirement, a decrease in the threshold current (I_{th}) and a concomitant increase in the slope efficiency (η_s) is necessary. In addition to the optimization of the waveguide design [4, 5] and that of the ridge etching [6, 7] to increase the confinement factor (Γ), another critical aspect for improving I_{th} deals with p-type doping since a lower [Mg] allows to inhibit the formation of compensating defects and non-uniform current injection into quantum wells (QWs) [8]. For III-N LDs operating at longer wavelength ($\lambda > 450$ nm), optimizing the growth temperature of the cladding layer is essential for minimizing or even avoiding the degradation of the QW gain medium [9, 10]. Besides, as will be shown hereafter, another possible way to decrease I_{th} while increasing η_s consists in reducing the cavity length as in this latter case, provided internal losses remain unaffected, the weight of mirror losses increases [11]. However, such a strategy can only be initiated at the expense of increasing challenges when processing devices. Previously, several groups have shown that shorter cavity LDs exhibit improved performance when it comes to the (I_{th}, η_s) combination [12, 13]. Nevertheless, the shortest reported III-N LD

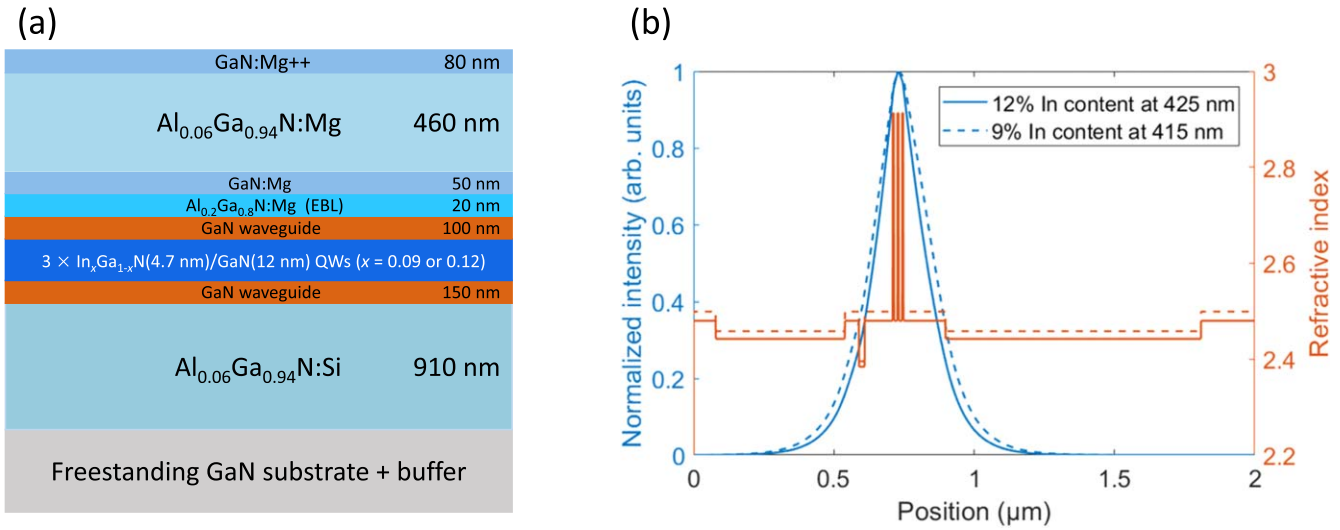

Figure 1. (a) Schematic cross-section (not to scale) of the as-grown LD structures. (b) Calculated mode profiles for the two sets of LD structures using a one-dimensional transfer matrix method (blue curves) and corresponding refractive index profiles (orange curves, with the sample surface on the left-hand side).

devices usually have a cavity length in the 400–600 μm range essentially due to processing and facet cleavage issues. Therefore, this is the aim of the present work to develop a reliable method to realize InGaN-based LDs of cavity length below 300 μm. To validate the adopted processing approach, the current–voltage ($I-V$) and light output ($L-I$) characteristics of such short cavity LDs were systematically investigated. Lasing is reported for edge emitting devices with two cavity configurations. In the first configuration, where only one facet is coated with a high-reflectivity (HR) dielectric distributed Bragg reflector (DBR), lasing in the continuous wave (cw) regime is obtained for structures down to 250 μm in length while lasing under pulsed injection is obtained for a cavity length as short as 100 μm. For the second configuration that relies on LD samples with their two facets coated with HR DBR, lasing in the cw regime is reported down to a cavity length as short as 45 μm.

Growth and fabrication details

LD structures were grown by metal organic vapor phase epitaxy in a vertical Aixtron 3 × 2 in. CCS reactor on 2 inch freestanding c-plane GaN substrates featuring a low dislocation density $\sim 10^6\,\mathrm{cm}^{-2}$. Following the deposition of an n-type doped GaN buffer, a 910 nm thick Si-doped (n-type) AlGaN cladding layer containing 6% of Al was grown ($n \sim 3 \times 10^{18}$ cm^{-3}). The active region consists of a 3-period $In_xGa_{1-x}N$(4.7 nm)/GaN(12 nm) QW with either $x = 0.09$ or 0.12 sandwiched between a 150 nm thick bottom GaN waveguide and a 100 nm thick top GaN waveguide. It is followed by a 20 nm thick $Al_{0.2}Ga_{0.8}N$ electron blocking layer (EBL), a 50 nm thick Mg-doped GaN layer, and a 460 nm thick Mg-doped $Al_{0.06}Ga_{0.94}N$ layer employed as p-type cladding. The net acceptor concentration ($N_A - N_D$) was measured by electrochemical capacitance–voltage ($C-V$) profiling and amounts to $\sim 1 \times 10^{19}\,\mathrm{cm}^{-3}$. The whole structure was finally capped by an 80 nm thick Mg-doped ($N_A - N_D \sim 2 \times 10^{19}$ cm^{-3}) GaN layer to favor the Ohmic contact for efficient hole injection. Figure 1(a) presents the detail of the whole structure. The fundamental transverse electric mode profile of the vertical waveguide at a wavelength of 415 nm ($x = 0.09$) and 425 nm ($x = 0.12$), respectively, was calculated by means of a one-dimensional transfer matrix model [14, 15]. In the simulation, the propagation constants of the eigenmodes were solved by matching the boundary conditions at all the interfaces and by requiring the field to converge at infinity. The refractive index (n_{op}) of GaN, InGaN, and AlGaN was taken from the work by Laws *et al* [16]. The calculated confinement factors amount to $\Gamma_{x=0.12} = 5.9\%$ at 425 nm and $\Gamma_{x=0.09} = 5.1\%$ at 415 nm, whose mode profiles are shown together with their corresponding refractive index profiles in figure 1(b).

After the growth, the wafers were processed into short cavity LDs. Due to inherent difficulties with the facet cleavage for cavity lengths (L_{cav}) shorter than 400 μm, the LDs were designed such that they each exhibit an etched facet and a cleaved facet. The etched facets (figure 2(b)) were obtained after the formation of 1.5 μm deep trenches using chlorine-based inductively coupled plasma (ICP) etching down to the n-type $Al_{0.06}Ga_{0.94}N$ cladding layer leading to 300 μm long initial cavity sections (see supplementary material (SM) section 1 available online at stacks.iop.org/SST/34/085005/mmedia for a description of the mask and subsequent explanation about the control of the cavity length). The etched facets were then smoothed in a KOH ethylene glycol (1:3) mixture solution for 20 min at 80 °C [17]. In order to precisely control the cavity length, 8 μm wide cleavage marks were also etched during this procedure. Subsequently, 3 μm wide laser ridges were etched by ICP (figure 2(c)) and coated with 300 nm of SiO_2 deposited by plasma-enhanced chemical vapor deposition (figure 2(d)). The LD structure was completed by the e-beam evaporation of a standard Pd(50 nm)/Au (400 nm) p-type Ohmic contact layer on the bare GaN ridge

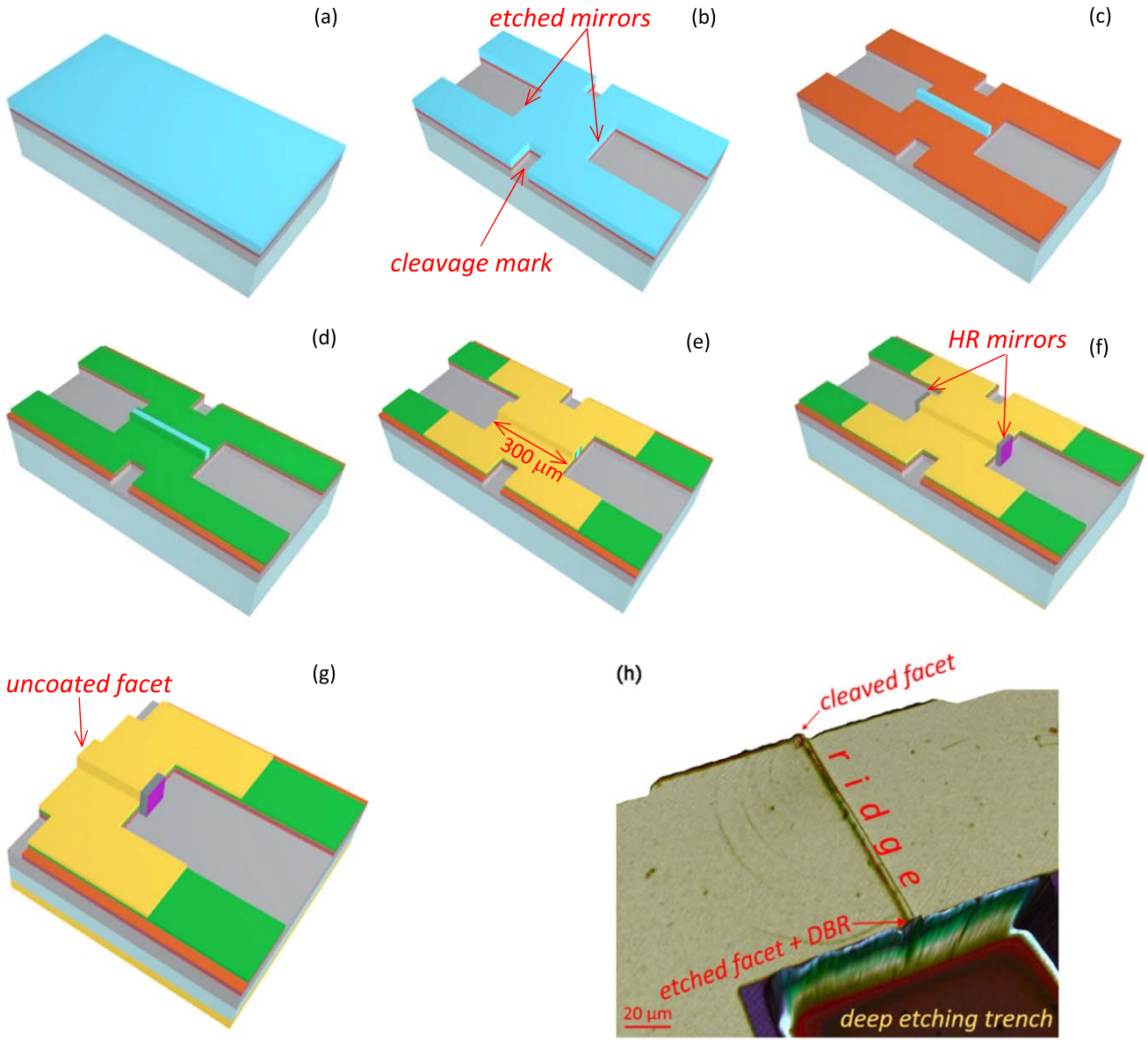

Figure 2. Schematic of the process flow: (a) as-grown sample, (b) 1.5 μm deep etching down to the *n*-type $Al_{0.06}Ga_{0.94}N$ cladding layer (gray) for realizing the etched facets and the cleavage marks, (c) ridge etching down to the upper part of the GaN waveguide (orange), (d) 300 nm thick SiO_2 encapsulation (green), (e) Pd/Au *p*-type contact deposition (gold) on the top surface including the bare GaN ridge, (f) HR SiO_2/ZrO_2 DBR mirror coating (purple) on the etched facets, (g) substrate grinding down to 100 μm, Ti/Al/Ti/Au *n*-type GaN contact deposition on the backside and laser ridge cleavage. (h) Tilted view confocal microscope image of a fully processed 100 μm long edge-emitting LD belonging to LD set 1.

(figure 2(e)). To reduce the impact of mirror induced losses, an eight pair SiO_2/ZrO_2 HR DBR was sputtered onto the two etched facets in a single deposition run using magnetron sputtering (figure 2(f)). More precisely, after depositing the *p*-type contact, a negative tone photoresist (nLOF 2020) was spin-coated followed by a photolithography step to expose the etched surface while leaving the rest of the sample protected by the photoresist. After patterning, the sample was transferred into the sputtering chamber and positioned in order to ensure homogeneous DBR mirror deposition on the etched facets. The samples were then immersed into a remover to liftoff the photoresist and finally obtain the structure shown in figure 2(f). Substrate grinding down to a thickness of 100 μm followed by e-beam evaporation of a Ti(10 nm)/Al(30 nm)/Ti(10 nm)/Au(200 nm) *n*-type Ohmic contact layer on the backside of the freestanding GaN wafer was then performed. Two sets of short cavity LDs were then finalized. LD set 1 corresponds to LDs with $In_{0.12}Ga_{0.88}N$/GaN QWs having a length after cleavage ranging from 290 down to 100 μm and a single HR DBR deposited on the etched facet. LD set 2 differs from LD set 1 by its gain medium that consists of three $In_{0.09}Ga_{0.91}N$/GaN QWs and the deposition of a second HR DBR on the cleaved facet at the very final stage of the LD process. The tolerance for each cavity length could be well controlled within 8 μm with the help of the above-mentioned alignment marks. Figure 2(g) represents a schematic view of a

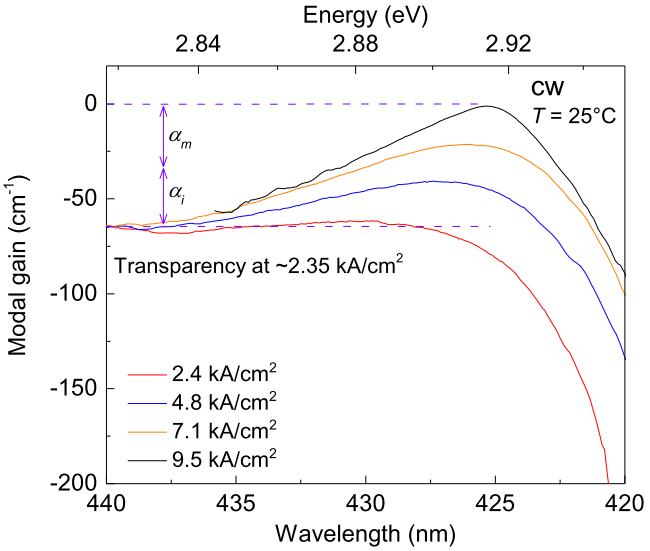

Figure 3. Modal gain spectra of a 280 μm long blue LD belonging to LD set 1 measured at current densities ranging from 2.4 up to 9.5 kA cm^{-2} using the Hakki–Paoli method.

fully processed short cavity LD while a tilted view confocal microscope image of such a fully processed 100 μm long LD belonging to LD set 1 is shown in figure 2(h).

Characterization of the processed laser diodes

To evaluate the quality of the HR DBRs, current density dependent modal gain spectra were measured on a 280 μm long device belonging to LD set 1 using the Hakki–Paoli (HP) method (figure 3) [18]. The related electroluminescence (EL) spectra were recorded by means of a Jobin-Yvon Triax 550 monochromator (55 cm focal length) equipped with a Symphony II liquid-N_2 cooled back-illuminated UV-enhanced charge-coupled device using a 2400 l mm^{-1} grating allowing for a spectral resolution of 38 pm. Transparency of the gain medium is reached at a current density (J_{th}) of 2.35 kA cm^{-2} as deduced from the flat band shape in the corresponding gain spectrum. With increasing current injection, the gain gradually counterbalances the losses and lasing eventually takes place when the modal gain compensates for the losses, which amount to ~62 cm^{-1}. Taking into account the value of internal losses, $\alpha_i \sim 30 \pm 2$ cm^{-1}, extracted from HP modal gain measurements performed on standard 600 μm long LDs (see SM section 2), mirror losses (α_m) are estimated to 32 $\pm$ 2 cm^{-1} for this sample, from which a peak reflectivity (R_{HR}) of 90 $\pm$ 7% is deduced for the coated HR mirror using $R = 0.18$ for the uncoated facet. This mirror reflectivity is close to the targeted value of 98% predicted by transfer matrix simulations, which also indicates the high quality of the etched mirror and the limited impact of undesired thickness fluctuations and/or short scale layer waviness.

To further characterize these 280 μm long cavity LDs, their electrical (I–V) and their optical properties were measured and are summarized in figures 4(a) and (b). The L–I characteristics was measured under both pulsed (1 kHz frequency with a 1% duty cycle) and cw injection at a regulated temperature of 25 °C by making use of a Peltier element. Under pulsed injection, these short LD devices exhibit lasing at a threshold current of 78 mA (i.e. 9.3 kA cm^{-2}). Above threshold, the output power increases abruptly up to a value of 20 mW at a current of 107 mA (12.7 kA cm^{-2}) leading to a slope efficiency (η_s) of 0.69 W/A. By making use of the equations.

$$\eta_i = \eta_s \frac{1}{F}\frac{q}{\hbar\omega}\frac{\alpha_i + \alpha_m}{\alpha_m}, \tag{1}$$

and

$$F = \frac{1 - R}{1 - R + \sqrt{R/R_{HR}}\,(1 - R_{HR})}, \tag{2}$$

where $\hbar\omega$ is the photon energy, q is the charge of the electron, and F is the fraction of power outcoupled from the uncoated facet [11], an injection efficiency (η_i) of 47 $\pm$ 3% was extracted assuming that the α_i and the η_i values deduced for the 600 μm LDs can still be used for the 280 μm LDs (see SM section 2). The L–I characteristics measured under cw injection shows similar features except for a slightly higher I_{th} value of 80 mA (9.5 kA cm^{-2}). The small difference observed between pulsed and cw operation indicates a fair p-type conductivity [19]. Figure 4(b) shows the evolution of the corresponding EL spectra as a function of current density.

To determine the role played by the cavity length on the (I_{th}, η_s) combination, the L–I characteristics were measured for the entire set of processed devices belonging to LD set 1. Representative characteristics among the lengths ranging between 250 and 290 μm, 150 and 200 μm, and 100 and 150 μm are displayed in figure 5. LD devices with a cavity length above 250 μm were measured under cw injection at 25 °C thanks to the efficient thermal management provided by the Peltier element whereas devices with a shorter cavity length were characterized under pulsed injection to avoid self-heating issues. From figure 5, we observe an increase in I_{th} from 85 mA (9.8 kA cm^{-2}) to 120 mA (23.5 kA cm^{-2}) and then up to 140 mA (46.7 kA cm^{-2}) for 290, 160 and 100 μm long LD devices, respectively. Let us note that the kinks observed in the L–I curves could potentially be due to lateral transverse mode instability as suggested by Lang [20]. However, such a detailed study goes beyond the scope of the present work.

The spacing between longitudinal modes ($\Delta\lambda$) was extracted from the EL spectra for different cavity lengths. With decreasing cavity length, $\Delta\lambda$ increases and amounts to 0.23 nm at 425 nm for the 120 μm long LDs (see inset of figure 5), a value in close agreement with the calculated value of 0.235 nm according to the equation

$$\Delta\lambda = \frac{\lambda^2}{2L_{cav}n_{op}}\left(1 - \frac{\lambda}{n_{op}}\frac{dn_{op}}{d\lambda}\right)^{-1}, \tag{3}$$

where we considered the refractive index of GaN [16]. Simultaneously, η_s values gradually reduce from 0.7 W/A for 290 μm long devices to 0.6 W/A for 160 μm long devices and finally down to 0.25 W/A for 100 μm long devices. Such

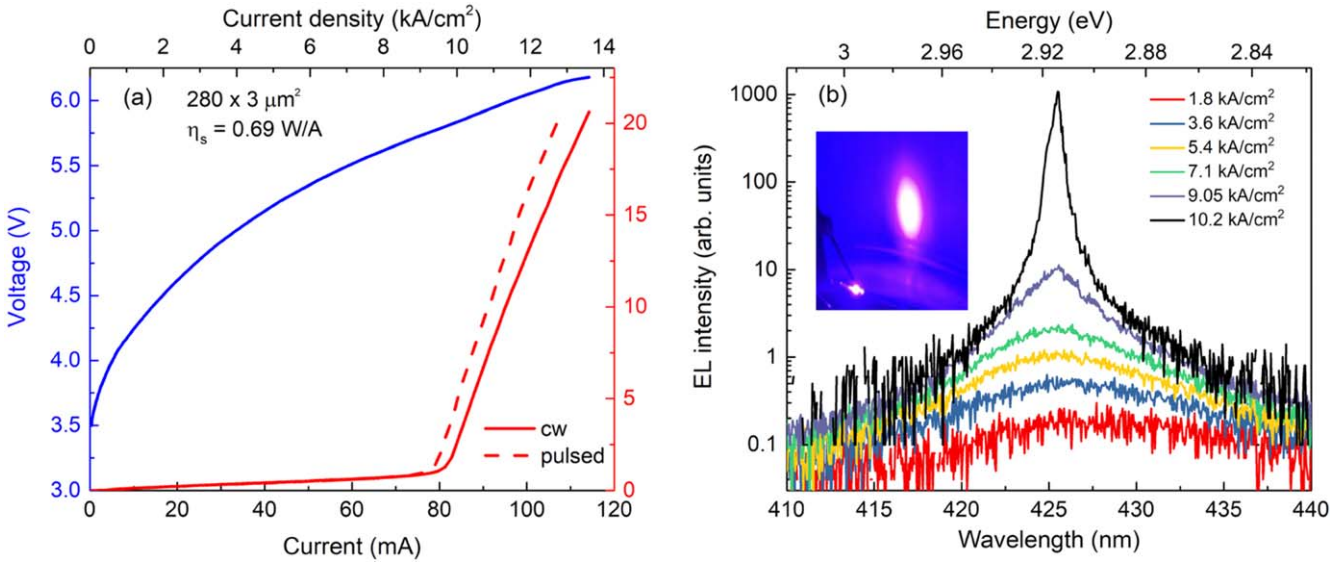

Figure 4. (a) $I-V$ and $L-I$ curves measured on a 280 μm long blue LD belonging to LD set 1 under both pulsed and cw injection, and (b) corresponding cw EL spectra. The inset shows the far-field emission pattern measured at a current density of 10.2 kA cm^{-2}.

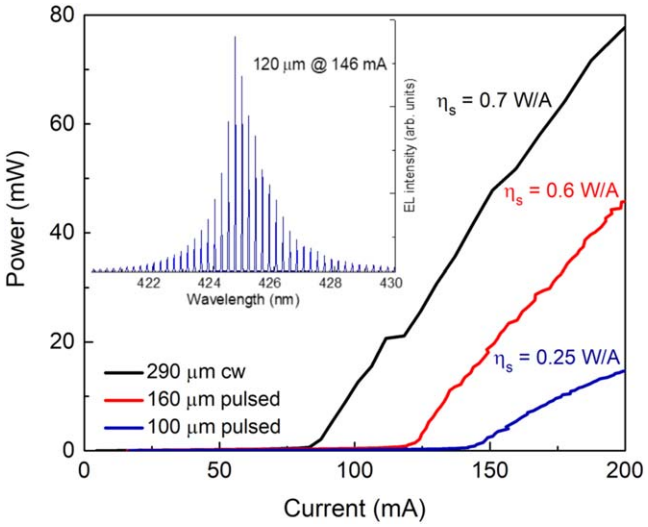

Figure 5. $L-I$ curves measured for 290, 160 and 100 μm long LDs of LD set 1. Inset: EL spectrum of a 120 μm long LD measured at 146 mA under pulsed injection.

a trend appears to be in contradiction with the initial statement made in the introduction and hence will be the subject of a discussion hereafter.

Besides, in order to further highlight the potential of such compact and hence low footprint edge emitting LDs, a few short edge emitting cavity devices made from LD set 2 with the rear and front facets each coated with an HR DBR were characterized. As for LD set 1, relevant information about losses and the injection efficiency was extracted from HP modal gain measurements performed on standard 400 μm long LDs (see SM section 2). Internal losses are somewhat lower in LD set 2 with a value amounting to 22 cm^{-1}. In figures 6(a) to (d), the $I-V$ and the $L-I$ curves measured on a 75 μm long and a 45 μm long device in the cw injection regime are displayed together with a representative EL spectrum measured slightly above threshold for each LD device. The 75 μm long LD exhibits a threshold current less than 10 mA with a value of 8.7 mA (i.e. $J_{th} = 3.9$ kA cm^{-2}) and a slope efficiency of 0.23 W/A, whereas the 45 μm long LD exhibits a threshold current of 13.8 mA (10.2 kA cm^{-2}) and a slope efficiency of 0.13 W/A. The mere fact that those sub-100 μm long devices operate in the cw regime clearly demonstrates the viability of the adopted processing scheme; even though the negative roll-over observed in the $L-I$ curve shown in figure 6(a) could be a manifestation of some non-uniform carrier injection due to the reduced size of the processed 75 μm long LD devices. Let us also note that the limited number of longitudinal modes in the EL spectra is commensurate with the short cavity length, which makes such LDs of interest for the realization of single mode edge emitting LDs, e.g. through the use of a superlattice made from a few short aperiodic grating sequences [21].

Discussion

To account for the physical origin behind the behavior of the (I_{th}, η_s) combination with decreasing cavity length observed for LD set 1, a comparison of the measured values with calculated ones as a function of cavity length was performed. The detail of the calculations is given in section 3 of the SM. In figure 7(a), the calculated threshold currents determined for various values of R_{HR} exhibit a smooth increase for cavity lengths shorter than 150 μm, which does coincide with the abrupt growth of J_{th} shown in figure 7(b). It is seen that the reported trend is weakly sensitive to the exact R_{HR} value in the limit of the high peak reflectivity regime for the coated facet (values in excess of 0.8). The increase occurring for relatively short cavity lengths is due to the logarithmic modal gain saturation and the concomitant decrease in the differential gain with decreasing cavity length [11]. Let us note

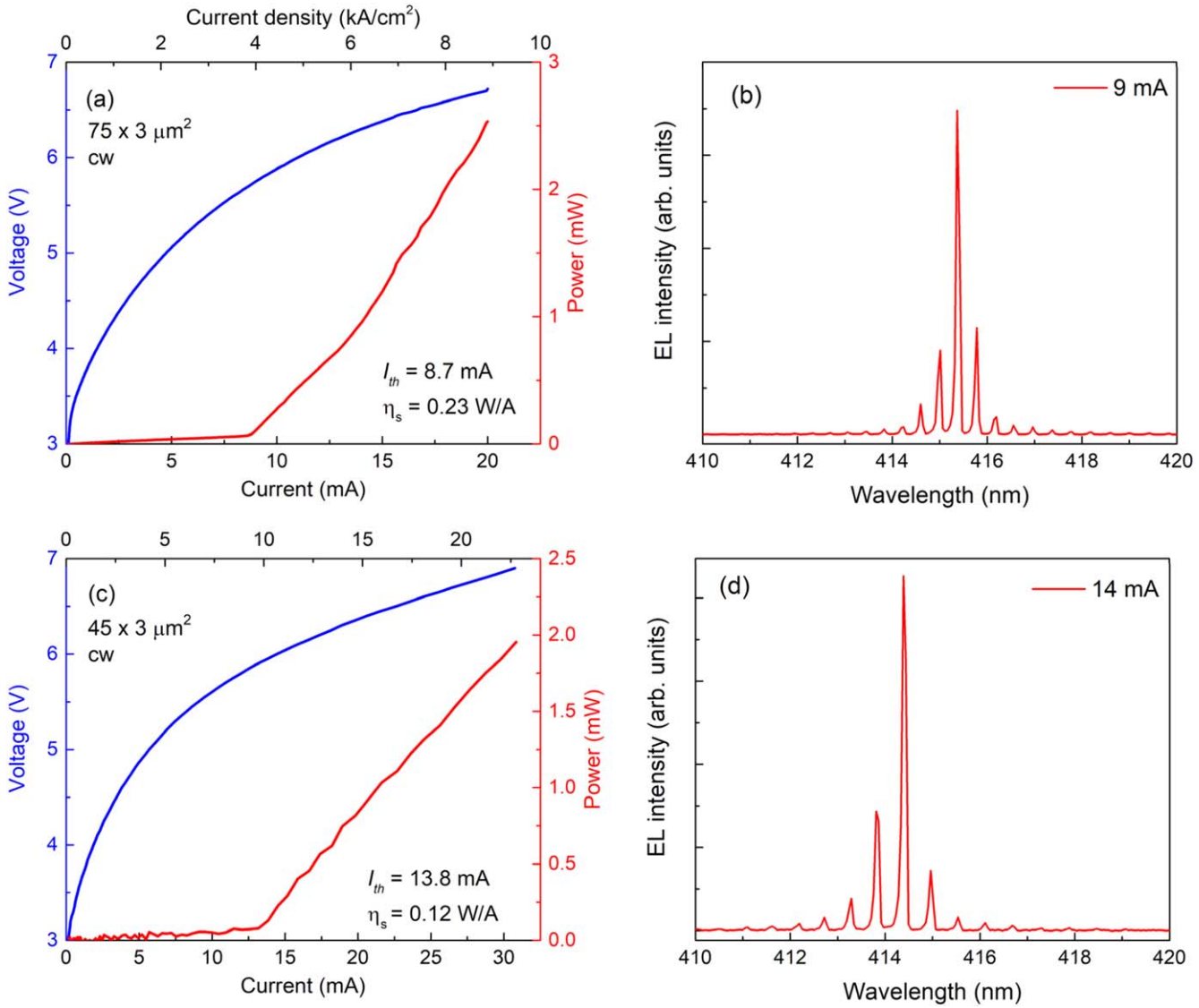

Figure 6. (a) $I-V$ and $L-I$ curves measured on a 75 μm long blue LD belonging to LD set 2 under cw injection and (b) corresponding cw EL spectrum. (c) $I-V$ and $L-I$ curves measured on a 45 μm long blue LD belonging to LD set 2 under cw injection and (d) corresponding cw EL spectrum.

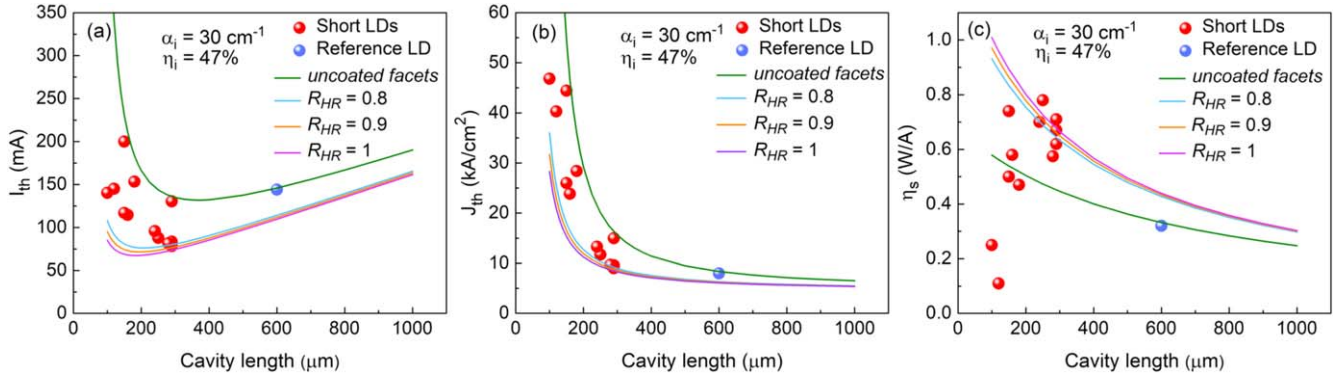

Figure 7. Measured (filled red dots for short LDs and filled blue dot for the 600 μm long reference LD) and calculated (continuous lines) (a) $I_{\rm th}$ values, (b) $J_{\rm th}$ values, and (c) η_s values as a function of cavity length for various $R_{\rm HR}$ values of LDs belonging to LD set 1. The linear part of the $L-I$ curves for output powers below 20 mW was considered to determine the η_s values.

however that this rise in I_{th} occurs at much larger cavity lengths for the fabricated LDs since a sharp increase of I_{th} values is visible for a cavity length of 270 μm. Indeed, the experimental increment amounts to $\Delta I_{th} \approx 60$ mA ($\Delta J_{th} \approx 30$ kA cm^{-2}) on average for $R_{HR} = 0.9$ and cavity lengths ranging between 290 and 100 μm compared to a calculated value $\Delta I_{th} \approx 23$ mA ($\Delta J_{th} \approx 20$ kA cm^{-2}). As far as η_s is concerned, a smooth increase is expected with decreasing cavity length together with an insensitivity to the R_{HR} value similar to that observed for I_{th} and J_{th} when R_{HR} exceeds 0.8. However, even though experimental results show a rise in the η_s values for cavity lengths ranging between 290 and 250 μm, a significant divergence is observed between experimental and calculated values for shorter cavity lengths as shown in figure 7(c). Such a behavior implies that the common assumption that α_i and η_i values remain constant and are thus unaffected by the cavity length is no longer valid for the present LDs when the ridge waveguide length is shorter than 250 μm. In order to reconcile calculations with experimental results we have to consider $\alpha_i > 30$ cm^{-1} and $\eta_i <$ 47%. Let us note that a quantitative estimate of the evolution of α_i and η_i lies beyond the scope of the present work. Nevertheless, a qualitative description for such a dependence upon decreasing cavity length can be inferred from the available literature on GaAs-based short cavity LDs [22, 23]. Indeed, in addition to increasing technical issues related to the fabrication of shorter and shorter LDs whose detrimental impact on the $I-V$ and the $L-I$ characteristics cannot be fully discarded, even though the results obtained on LD set 2 indicates the viability of the adopted processing scheme, the shorter the ridge waveguide length, the higher J_{th} and consequently the higher the clamped carrier density. In this latter case, residual absorption due to free carriers could be at play as suggested by first-principles calculations that emphasized the peculiar detrimental impact of phonon-assisted absorption by holes occurring in the p-type layer [24]. A side consequence of the larger clamped carrier density is the increased weight of Auger recombination, which is responsible for a shorter Auger-related carrier lifetime [25, 26]. It is known to be accompanied by a decrease in η_r -the so-called recombination losses- due to nonuniform carrier distribution across the QWs, whose impact for short cavity devices is more prominent than for longer devices due to the larger clamped carrier density, that can ultimately impact the slope efficiency (see SM section 4 for a detailed account about this aspect) [23, 27]. Hence the above-mentioned effects are likely candidates for explaining the concomitant increase in I_{th} and the decrease in η_s with decreasing cavity length. A table summarizing the main features of the short cavity LDs described in this work as well as those of the reference devices for LD sets 1 and 2 is shown in section 5 of the SM.

Beyond the present proof of principle, which illustrates the high potential of the III-nitride platform for the realization of low footprint edge emitting LDs most likely due to its large modal gain, we can mention that the further optimization of the $I-V$ and the $L-I$ characteristics of such devices would require the tuning of several parameters as already demonstrated with the well-established GaAs and InP platforms [11]. In order to bring I_{th} and J_{th} values further toward the bottom left corner of figures 7(a) and (b) and η_s values toward the top left corner of figure 7(c), the most obvious parameters to play with are the number of QWs as well as their width and the ridge stripe width [28, 29]. Let us note that in order to further mitigate the detrimental impact of the Auger term on I_{th} [11], the use of an indium containing underlayer [30] in the bottom cladding region would certainly prove highly beneficial, in particular short period InAlN/(Al)GaN superlattices that have a low refractive index would be especially suited [31]. This is motivated by the recent demonstration of the link existing between the Shockley–Read–Hall (A) and the Auger (C) coefficients that highlighted that the larger A, the larger C [32]. Hence limiting the weight of those coefficients should prove valuable even in the high carrier density regime.

Conclusion

In conclusion, we demonstrated cw lasing at ~425 nm in edge-emitting LD structures that consist of one uncoated cleaved facet and one etched facet coated with an HR DBR for cavity lengths down to 250 μm with η_s values in excess of 0.6 W/A, while lasing was observed under pulsed injection for a length as short as 100 μm. When switching to structures with a second HR dielectric DBR, we could demonstrate cw lasing at ~415 nm for a cavity length as short as 45 μm with a threshold current below 10 mA being reported for a 75 μm long device. By monitoring the current–voltage and light output characteristics of short cavity edge emitting LDs consisting of one uncoated cleaved facet and one etched facet with a highly reflective coating, we observed a marked increase in I_{th} and a decrease in η_s when the cavity length is shortened from 300 down to 100 μm. Such counterintuitive behavior is ascribed to the likely increase of internal losses originating from free carriers and the concomitant degradation of the internal quantum efficiency due to the larger weight of Auger processes together with the decrease in the recombination losses due to nonuniform carrier distribution across the QW active region. Beyond the demonstration of lasing in short emitting devices at blue wavelengths, in a regime of high threshold carrier density of interest for better understanding the gain mechanisms in such devices, this work highlights the potential of III-nitrides for the practical realization of low footprint coherent light emitting devices with high slope efficiency that could also become a viable alternative to blue vertical cavity surface emitting lasers.

Funding

This work was supported by EU Horizon H2020 project SUPERTWIN (id686731).

ORCID iDs

Raphaël Butté https://orcid.org/0000-0002-8474-217X

References

[1] Akasaki I 2015 Nobel Lecture: fascinated journeys into blue light *Rev. Mod. Phys.* **87** 1119–31

[2] Amano H 2015 Nobel Lecture: growth of GaN on sapphire via low-temperature deposited buffer layer and realization of $p-$ type GaN by Mg doping followed by low-energy electron beam irradiation *Rev. Mod. Phys.* **87** 1133–8

[3] Nakamura S 2015 Nobel Lecture: Background story of the invention of efficient blue InGaN light emitting diodes *Rev. Mod. Phys.* **87** 1139–51

[4] Castiglia A, Feltin E, Cosendey G, Altoukhov A, Carlin J-F, Butté R and Grandjean N 2009 $Al_{0.83}In_{0.17}N$ lattice-matched to GaN used as an optical blocking layer in GaN-based edge emitting lasers *Appl. Phys. Lett.* **94** 193506

[5] Kawaguchi M, Imafuji O, Nozaki S, Hagino H, Takigawa S, Katayama T and Tanaka T 2016 Optical-loss suppressed InGaN laser diodes using undoped thick waveguide structure *Proc. SPIE* **9748** 974818

[6] Schwarz U T, Pindl M, Sturm E, Furitsch M, Leber A, Miller S, Lell A and Härle V 2005 Influence of ridge geometry on lateral mode stability of (Al, In)GaN laser diodes *Phys. Status Solidi* a **202** 261–70

[7] Zhang L Q, Jiang D S, Zhu J J, Zhao D G, Liu Z S, Zhang S M and Yang H 2009 Confinement factor and absorption loss of AlInGaN based laser diodes emitting from ultraviolet to green *J. Appl. Phys.* **105** 023104

[8] Castiglia A, Rossetti M, Matuschek N, Rezzonico R, Duelk M, Vélez C, Carlin J-F and Grandjean N 2016 GaN-based superluminescent diodes with long lifetime *Proc. SPIE* **9748** 97481V

[9] Malinverni M *et al* 2015 InGaN laser diodes emitting at 500 nm with $p-$ layers grown by molecular beam epitaxy *Appl. Phys. Express* **8** 022105

[10] Li Z *et al* 2013 Suppression of thermal degradation of InGaN/GaN quantum wells in green laser diode structures during the epitaxial growth *Appl. Phys. Lett.* **103** 152109

[11] Coldren L A and Corzine S W 1995 *Diode Lasers and Photonic Integrated Circuits* (New York: Wiley)

[12] Ryu H Y *et al* 2008 Determination of internal parameters in blue InGaN laser diodes by the measurement of cavity-length dependent characteristics *Appl. Phys. Lett.* **93** 011105

[13] Becerra D L, Kuritzky L Y, Nedy J, Abbas A S, Pourhashemi A, Farrell R M, Cohen D A, DenBaars S P, Speck J S and Nakamura S 2016 Measurement and analysis of internal loss and injection efficiency for continuous-wave blue semipolar (20 $\overline{2}\overline{1}$) III-nitride laser diodes with chemically assisted ion beam etched facets *Appl. Phys. Lett.* **108** 091106

[14] Bergmann M J and Casey H C Jr. 1998 Optical-field calculations for lossy multiple-layer $Al_xGa_{1-x}N/In_xGa_{1-x}N$ laser diodes *J. Appl. Phys.* **84** 1196–203

[15] Rumpf R C 2011 Improved formulation of scattering matrices for semi-analytical methods that is consistent with convention *Prog. Electromagn. Res.* B **35** 241–61

[16] Laws G M, Larkins E C, Harrison I, Molloy C and Somerford D 2001 Improved refractive index formulas for the $Al_xGa_{1-x}N$ and $In_yGa_{1-y}N$ alloys *J. Appl. Phys.* **89** 1108–15

[17] Böttcher T, Zellweger C, Figge S, Kröger R, Petter C, Bühlmann H-J, Ilegems M, Ryder P L and Hommel D 2002 Realization of a GaN laser diode with wet etched facets *Phys. Status Solidi* a **191** R3–5

[18] Hakki B W and Paoli T L 1975 Gain spectra in GaAs double-heterostructure injection lasers *J. Appl. Phys.* **46** 1299–306

[19] Kuramata A, Kubota S-I, Soejima R, Domen K, Horino K and Tanahashi T 1998 Room-temperature continuous wave operation of InGaN laser diodes with vertical conducting structure on SiC substrate *Japan. J. Appl. Phys.* **37** L1373–5

[20] Lang R 1979 Lateral transverse mode instability and its stabilization in stripe geometry injection lasers *IEEE J. Quantum Electron.* **15** 718–26

[21] Blanchard R, Menzel S, Pflügl C, Diehl L, Wang C, Huang Y, Ryou J-H, Dupuis R D, Dal Negro L and Capasso F 2011 Gratings with an aperiodic basis: single-mode emission in multi-wavelength lasers *New J. Phys.* **13** 113023

[22] Chen T R, Eng L, Zhao B, Zhuang Y H, Sanders S, Morkoç H and Yariv A 1990 Submilliamp threshold InGaAs-GaAs strained layer quantum-well laser *IEEE J. Quantum Electron.* **26** 1183–90

[23] Piprek J, Abraham P and Bowers J E 1999 Carrier nonuniformity effects on the internal efficiency of multiquantum-well lasers *Appl. Phys. Lett.* **74** 489–91

[24] Kioupakis E, Rinke P and Van de Walle C G 2010 Determination of internal loss in nitride lasers from first principles *Appl. Phys. Express* **3** 082101

[25] Shahmohammadi M, Liu W, Rossbach G, Lahourcade L, Dussaigne A, Bougerol C, Butté R, Grandjean N, Deveaud B and Jacopin G 2017 Enhancement of Auger recombination induced by carrier localization in InGaN/GaN quantum wells *Phys. Rev.* B **95** 125314

[26] Scheibenzuber W G, Schwarz U T, Sulmoni L, Dorsaz J, Carlin J-F and Grandjean N 2011 Recombination coefficients of GaN-based laser diodes *J. Appl. Phys.* **109** 093106

[27] Piprek J, Abraham P and Bowers J E 1999 Cavity length effects on internal loss and quantum efficiency of multiquantum-well lasers *IEEE J. Sel. Top. Quantum Electron.* **5** 643–7

[28] Hu S Y, Corzine S W, Law K K, Young D B, Gossard A C, Coldren L A and Merz J L 1994 Lateral carrier diffusion and surface recombination in InGaAs/AlGaAs-quantum-well ridge-wave-guide-lasers *J. Appl. Phys.* **76** 4479–87

[29] Heimbuch M E, Holmes A L Jr., Reaves C M, Mack M P, DenBaars S P and Coldren L A 1994 Tertiarybutylarsine and tertiarybutylphosphine for the MOCVD growth of low-threshold 1.55μm $In_yGa_{1-y}As/InP$ quantum-well lasers *J. Electron. Mater.* **23** 87–91

[30] Haller C, Carlin J-F, Jacopin G, Liu W, Martin D, Butté R and Grandjean N 2018 GaN surface as the source of non-radiative defects in InGaN/GaN quantum wells *Appl. Phys. Lett.* **113** 111106

[31] Haller C, Carlin J-F, Mosca M, Rossell M D, Erni R and Grandjean N 2019 InAlN underlayer for near ultraviolet InGaN based light emitting diodes *Appl. Phys. Express* **12** 034002

[32] David A, Young N G, Hurni C A and Craven M D 2019 Quantum efficiency of III-nitride emitters: evidence for defect-assisted nonradiative recombination and its effect on the green gap *Phys. Rev. Appl.* **11** 031001